

# Soft Interaction Processes at HERA: Leading Baryon Production, Multi-Parton Interactions

Armen Bunyatyan

DESY, Notkestrasse 85, 22607 Hamburg, Germany

(for the H1 and ZEUS Collaborations)

DOI: will be assigned

Experimental results from HERA on the production of leading protons and neutrons in  $ep$  collisions are reviewed. The measurements are well described by the models which include virtual meson exchange. Assuming the validity of pion exchange model, the leading neutron data are used to constrain the pion structure function. A refinement of the simple factorisation picture is provided by baryon absorption, occurring through rescattering. Exchange models accounting for absorption describe the  $Q^2$  evolution of the data.

Furthermore, the influence of underlying event and multi-parton interactions on the charged particle multiplicity in the photoproduction of jets is investigated.

## 1 Introduction

The QCD hardness scale for secondary particles production in semiinclusive deep inelastic scattering (DIS) gradually decreases from  $Q^2$ , the photon virtuality which determines the hard scale in the virtual photon (current) fragmentation region, to a soft, hadronic, scale in the proton fragmentation region. Production of leading baryons (LB) in a process with a hard scale provides a probe of the relationship between the QCD of quarks and gluons and the strong interaction of hadrons. The LBs are produced with small transverse momentum  $p_T$ , ensuring the presence of a soft process with its related long-range correlations.

The observation of events with neutrons or protons carrying a large fraction  $x_L$  of the incident proton beam energy in electron-proton scattering at HERA [1–6] has led to renewed interest in the QCD evolution and factorisation properties of proton fragmentation to LBs in DIS [7–18].

Although a fraction of these LBs may result from the hadronisation of the proton remnant, the  $t$ -channel exchange of colour singlet virtual particles is expected to contribute significantly [7, 8, 19, 20]. In this picture, the proton fluctuates into a virtual meson-baryon state; the virtual photon subsequently interacts with a parton from the pion, leaving a fast forward baryon in the final state (figure 1). The production of leading neutron (LN) in the virtual ex-

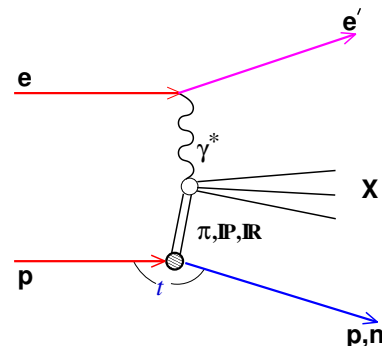


Figure 1: Leading baryon production via the colour singlet exchange processes.

change model occurs through the exchange of isovector states, and  $\pi^+$  exchange is expected to dominate. For leading proton (LP) production, isoscalar exchanges also contribute, including diffractive Pomeron mediated interactions. In the simple exchange picture, the cross section is factorised and LB production is largely independent of the variables describing the photon vertex (vertex factorisation). For example, if pion exchange dominates LN production, the cross section can be written as  $d\sigma_{\gamma^*p \rightarrow nx} = f_{\pi/p}(x_L, t) \times d\sigma_{\gamma^*\pi \rightarrow X}$ . Here  $f_{\pi/p}$  is the flux of virtual pions in the proton, a factor constrained from low energy hadronic data. Such a reaction can thus be used to probe the structure function  $F_2^\pi$  of the exchanged pion.

The H1 and ZEUS experiments measured leading baryons in DIS and photoproduction events. Leading protons were measured with position sensitive detectors placed along the proton beam downstream of the interaction point. Leading neutrons were measured with lead-scintillator forward calorimeters at the zero-degree point after the proton beam was bent vertically; magnet apertures limited neutron detection to scattering angles less than 0.75 mrad.

## 2 Leading baryon production cross sections and models

Figure 2 shows the cross sections of LP and LN production in DIS [4, 6] normalised to the inclusive DIS cross section as function of  $x_L$ . For LPs, the rate is approximately flat up to the diffractive peak, where it increases by a factor of about six. For LNs, the cross section rises from the lowest  $x_L$  due to the increase in  $p_T^2$  space, reaches a maximum near  $x_L = 0.7$ , and falls to zero at  $x_L = 1$ . The right side of figure 2 shows a comparison of normalised LP and LN cross sections restricted to the same  $p_T^2$  range of  $p_T^2 < 0.04 \text{ GeV}^2$ . In the range  $0.32 < x_L < 0.92$ , there are approximately twice as many protons as neutrons. In a particle exchange model, the exchange of isovector particles would result in half as many protons as neutrons. Thus, exchange of isoscalars must be invoked to account for the observed proton rate.

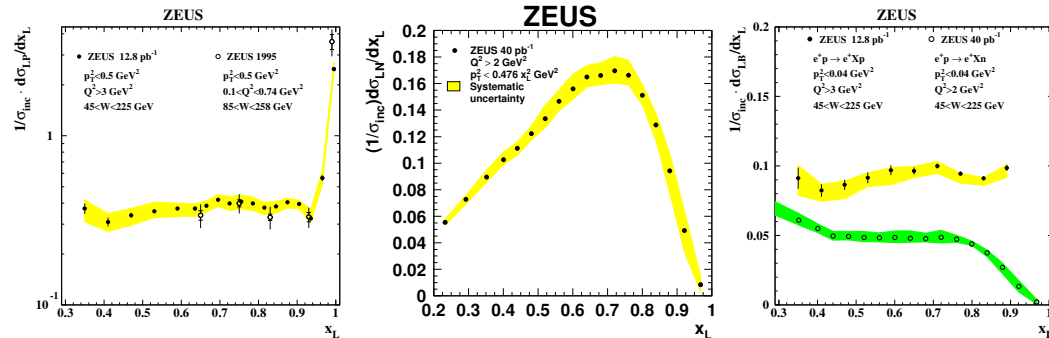


Figure 2: The distributions  $(1/\sigma_{inc})d\sigma_{LB}/dx_L$  for protons (left) and neutrons (central) in DIS. The right side figure shows the comparison of leading proton and neutron  $x_L$  spectra to restricted range in  $p_T^2 < 0.04 \text{ GeV}^2$ .

Figure 3 shows the double differential cross-section for LN and LP production in DIS as a function of  $p_T^2$  in bins of  $x_L$ , normalised to the inclusive DIS cross section. In each  $x_L$  bin the data are well described by an exponential distribution  $a(x_L) \cdot e^{-b(x_L)p_T^2}$ . The LN  $x_L$  cross section, the intercepts  $a$  and slopes  $b$  are compared in figure 4 to several Monte Carlo (MC) models [21, 22]. None of the models incorporating only standard fragmentation predicts the

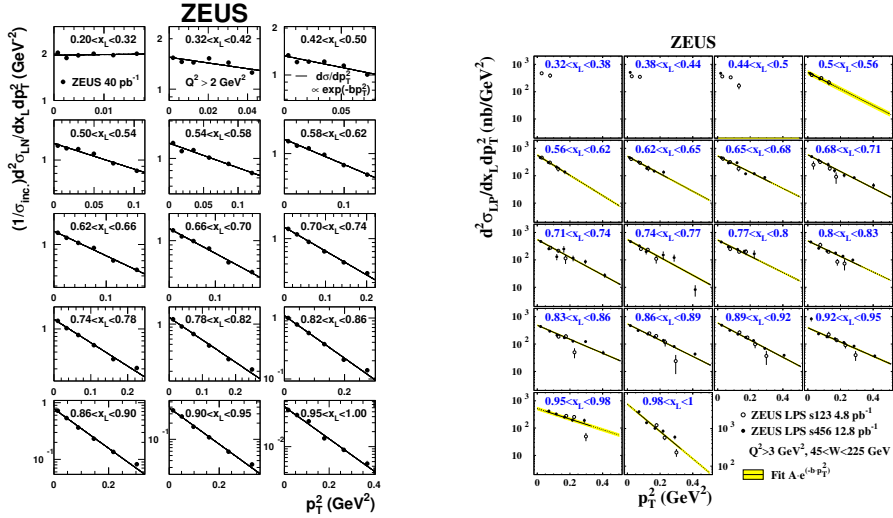


Figure 3: LN and LP cross-sections in DIS as function of  $p_T^2$  in bins of  $x_L$ , normalised to the inclusive DIS cross section. Lines are the results of fits to an exponential function.

observed LN yield [4, 5]. The mixture of the standard fragmentation and  $\pi$ -exchange models gives a better description of the shape of the  $x_L$  distribution, and also predicts the rise of  $b$  with  $x_L$ , although with too high values.

A similar failure to describe the data is observed for LP production in DIS [6]. Left side of figure 5 shows a comparison of the  $x_L$  distribution and the  $p_T^2$  exponential slope  $b$  to the predictions of MC models. None of them can reproduce either the flat dependence of the cross section versus  $x_L$  below the diffractive peak at  $x_L = 1$  or the magnitude and dependence of  $b$  on  $x_L$ . The same data are compared in right side of figure 5 to a Regge-based model [10] incorporating the isovector and isoscalar exchanges, and including the Pomeron for diffraction. A good description of the  $x_L$  distribution and the slopes is obtained by adding a substantial contribution of isoscalar Reggeon exchanges, which turn out to be the dominant processes below the diffractive peak.

### 3 Vertex factorisation and absorptive effects

A refinement of the simple factorisation picture is provided by baryon absorption, which can occur through rescattering [16–18]. In a geometrical picture [17], if the size of the meson-baryon system is small compared to the size of the photon, the baryon may also scatter on the photon and migrate to lower  $x_L$  or higher  $p_T$ , thus escaping detection. This results in a relative depletion of observed forward baryons. Since the size of the photon is inversely related to the photon virtuality  $Q^2$ , more absorption is expected in photoproduction ( $Q^2 \sim 0$ ) than in DIS. Also, since the size of the meson-baryon system is inversely proportional to the baryon  $p_T$ , rescattering results in a depletion of high  $p_T$  baryons in photoproduction relative to DIS.

To investigate the  $Q^2$  dependence of LN production, the  $x_L$  distributions for photoproduction and for DIS in three bins of increasing  $Q^2$  are shown in left side figure 6. The yield of LNs decreases monotonically with decreasing  $Q^2$ . This is in qualitative agreement with the

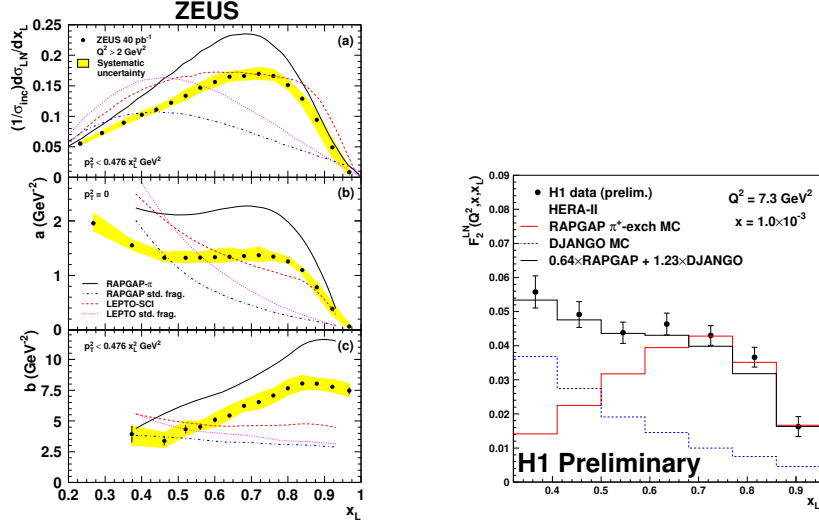


Figure 4: Left: Normalised LN cross section, intercept  $a$  and exponential slope  $b$  as function of  $x_L$ , compared to Monte Carlo models. Right: LN  $x_L$  distribution with an optimised mixture of exchange and fragmentation models.

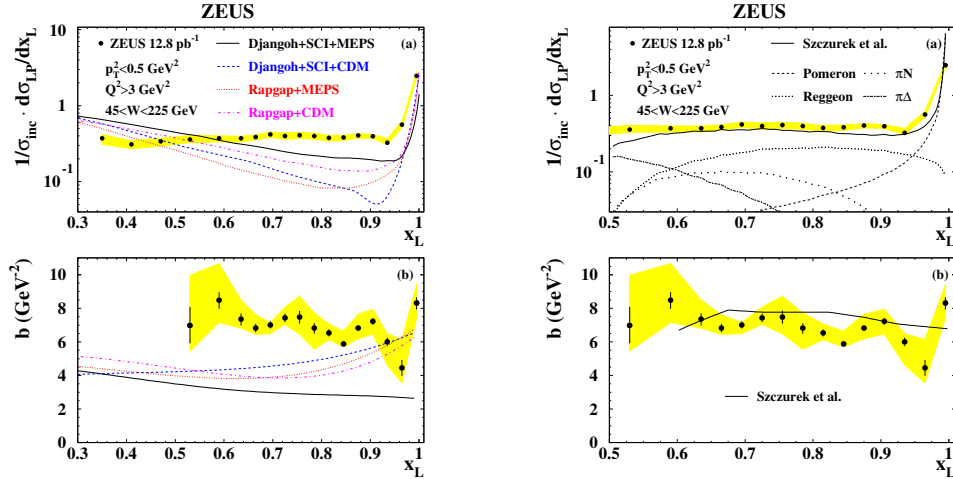


Figure 5: Normalised LP cross section and exponential slope  $b$  of LPs in DIS as function of  $x_L$ , compared to Monte Carlo models (left) and a Regge-based model [10] (right).

expectations of an increase of absorption as  $Q^2$  decreases. A similar  $Q^2$  dependence of the yields also observed in the LP data [4]

A calculation of LN production through pion exchange with neutron absorption, based on multi-pomeron exchanges, has become available [18]. It also accounts for the migration of the neutrons in  $x_L$  and  $p_T$  after rescattering and includes secondary exchanges of  $\rho$  and  $a_2$  mesons. The prediction of this model for the  $x_L$  neutron distribution in photoproduction is shown in right side of figure 6. A fair description of both the shape and the magnitude of the

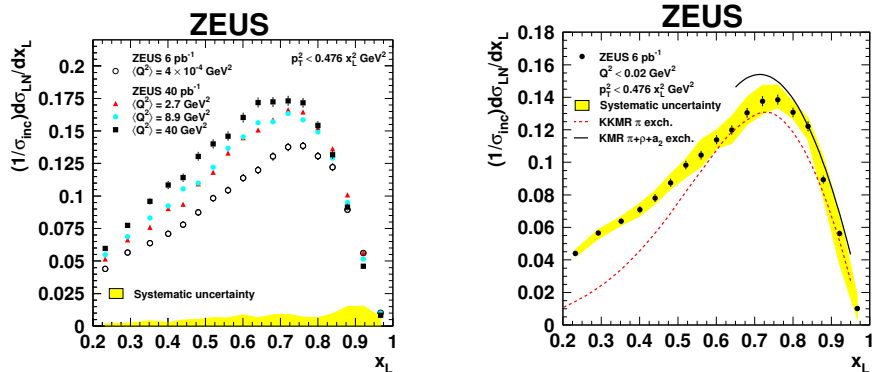


Figure 6: Left: normalised LN cross section as function of  $x_L$  for photoproduction and for three bins of  $Q^2$  in DIS. Right: LN  $x_L$  distribution for photoproduction compared to exchange models including absorption effects.

distribution is observed. However, the model with pion exchange predicts higher value of the slope  $b$ . Extending the model to include also secondary exchanges, a better description of the observed slopes is obtained still while maintaining a fair description of the  $x_L$  distribution.

## 4 Leading neutron production and the pion structure function

Analogous to the inclusive proton structure function  $F_2(x, Q^2)$ , the semi-inclusive LN structure function  $F_2^{LN(3)}(x, Q^2, x_L)$  is defined as

$$\frac{d^3\sigma}{dQ^2 dx dx_L} = \frac{4\pi\alpha^2}{xQ^4} \left[1 - y + \frac{y^2}{2}\right] \cdot F_2^{LN(3)}(x, Q^2, x_L).$$

Figure 7 shows the ratios  $F_2^{LN(3)}/F_2$  in bins of  $x$  and  $x_L$  as a function of  $Q^2$  [5], where  $F_2^{LN}$  values are measured from LN production in DIS, and  $F_2$  is obtained from the H1 PDF 2000 parameterisations [23]. At fixed  $x_L$ , ratios are almost flat in all  $(x, Q^2)$  bins, suggesting the validity of vertex factorisation, i.e. independence of the photon and proton vertices.

Assuming that the pion exchange dominates the LN production at high  $x_L$ ,  $F_2^{LN}$  can be presented as a product of a pion flux factor  $f_{\pi/p}(x_L, t)$  and the pion structure function  $F_2^\pi(\beta, Q^2)$ , where  $\beta = x/(1 - x_L)$  is the fraction of the pion momentum carried by the struck parton. The parton distributions in the pion have been previously constrained from Drell-Yan processes and direct photon production in pion-nucleon collisions, and are limited to high  $\beta$  ( $\gtrsim 0.1$ ) values. This measurement of  $F_2^{LN(3)}$  allows to test these parameterisations at lower  $\beta$ . The pion structure function can be estimated as  $F_2^\pi = F_2^{LN}/\Gamma_\pi$ , where  $\Gamma_\pi$  is the integrated over  $t$  pion flux. The value of  $\Gamma_\pi$  depends on pion flux parameterisation: for the parameterisation from [7],  $\Gamma_\pi = 0.131$ . The right side of figure 7 shows  $F_2^{LN}/\Gamma_\pi$  as a function of  $\beta$  for fixed values of  $Q^2$ . The data are compared to the two parameterisations of the pion structure function [24, 25] as well as to the H1 PDF 2000 [23] parameterisation of the proton structure function scaled by the factor  $2/3$ , according to the naive expectation based on the number of valence quarks in

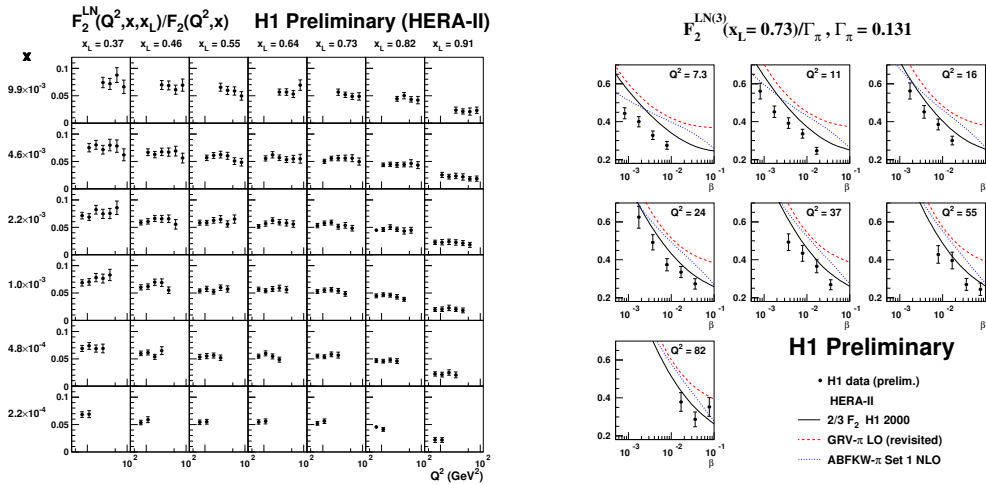


Figure 7: Left: ratio of the semi-inclusive LN to inclusive structure functions as a function of  $Q^2$  in bins of  $x$  and  $x_L$ . Right: The semi-inclusive LN structure function  $F_2^{LN(3)}$  divided by the integrated pion flux plotted as function of  $\beta = x/(1-x_L)$  in bins of  $Q^2$ . The curves are the proton structure function scaled by 2/3 and two parameterisations of pion structure function.

the pion and the proton respectively. The measured data show a steep rise with decreasing  $\beta$ , in accordance with  $F_2^\pi$  parameterisations, but are slightly below the expectations, suggesting that additional phenomena, like absorption, may play a role. Also, the theoretical uncertainties on the pion flux factor need to be carefully considered before any conclusion can be drawn.

## 5 Study of Multiple Interactions in photoproduction

The phenomena of absorption and rescattering discussed above are closely related to the multiparton interactions (MI) which play an important role in hadronic interactions. The MI take place when the density of partons in the colliding beams is large enough that more than one interaction happens within one collision. MI have been required to describe the transverse momentum and particle multiplicity distributions in a region transverse to the jets at the TeVatron. In quasi-real photoproduction ( $Q^2 \sim 0$ ) the photon has a point-like as well as a hadronic (resolved) component. Measurements in photoproduction at HERA have the advantage that the transition from a point-like photon towards a resolved photon can be studied in detail as function of the variable  $x_\gamma$ . MI are expected within the model of [26, 27] for resolved photons ( $x_\gamma < 1$ ) but not for the point-like photons which have  $x_\gamma = 1$ .

In the photoproduction of dijets at HERA the effects of MI and underlying event can be studied in a fashion similar to the studies done at the TeVatron [28]. The underlying event is defined as everything in addition to the dijet production and includes MI as well as the contributions coming from higher order QCD radiation and hadronisation. The average track multiplicity as a function of the difference in azimuthal angle  $\Delta\phi = \phi_{jet} - \phi_{track}$  is shown in figure 8 for the two  $x_\gamma$  regions: a resolved photon enriched region with  $x_\gamma < 0.7$  and a point-like photon enriched region with  $x_\gamma > 0.7$  [29]. The contributions from leading, subleading and

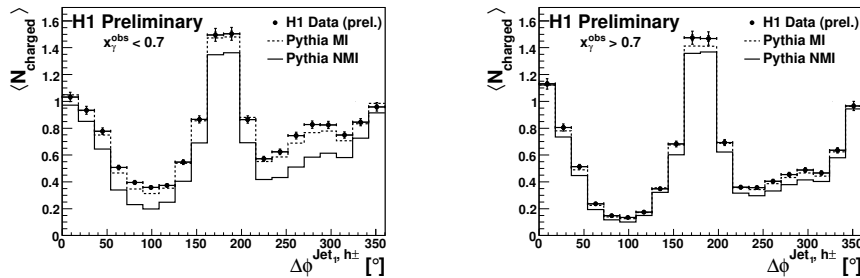


Figure 8: Charged particle multiplicity as a function of the difference in azimuthal angle  $\Delta\phi = \phi_{jet} - \phi_{track}$  for  $x_\gamma < 0.7$  (left) and for  $x_\gamma > 0.7$  (right). Data is compared to PYTHIA MC predictions with and without multi-parton interactions.

third jets are clearly visible. The data are compared to predictions of PYTHIA MC [27]. For large  $x_\gamma$  the effect of MI is very small, while at  $x_\gamma < 0.7$  the inclusion of MI contributes as a pedestal to the track multiplicity and improves the description of the data.

In figure 9 the average charge particle multiplicity is shown for the transverse regions of leading and subleading jets (*toward* and *away* regions). In general, the average track multiplicity rises with increasing  $P_T^{Jet}$  from around 4-5 particles at  $P_T^{Jet} \sim 5 \text{ GeV}$  to around 7 particles at higher  $P_T^{Jet}$  depending on  $x_\gamma$ . In the region of  $x_\gamma > 0.7$  the measurements are reasonably well described with a simulation containing only one hard interaction together with parton showers and hadronisation, whereas at low  $x_\gamma$  good agreement is achieved only if MI are included in the simulation. The simulation including MI gives also a reasonable description of the average charged particle multiplicity in the transverse region over the full phase space region.

## 6 Conclusions

The presence of a leading baryon in the final state provides information on the relationship between the soft and hard aspects of the strong interaction. The production of leading baryons has been studied as a function of several kinematic variables. There is a clear evidence that both contributions from fragmentation processes and from the exchange of colour-neutral particles such as isoscalars are required to describe the data. Thus the data show sensitivity to fragmentation models. With the assumption that pion exchange dominates leading neutron production the leading neutron data is sensitive to the pion structure function.

The charged particle multiplicity is studied in the photoproduction of jets. The measurements is described by PYTHIA simulation which includes multi-parton interactions.

## References

- [1] C. Adloff *et al.* [H1 Collaboration], Eur. Phys. J. **C6** (1999) 587, [hep-ex/9811013].
- [2] S. Chekanov *et al.* [ZEUS Collaboration], Nucl. Phys. **B637** (2002) 3, [hep-ex/0205076].
- [3] A. Aktas *et al.* [H1 Collaboration], Eur. Phys. J. **C41** (2005) 273, [hep-ex/0501074].
- [4] S. Chekanov *et al.* [ZEUS Collaboration], Nucl. Phys. **B776** (2007) 1, [hep-ex/0702028].
- [5] H1 Collaboration, “Leading Neutron production in DIS at HERA”, H1prelim-08-111.

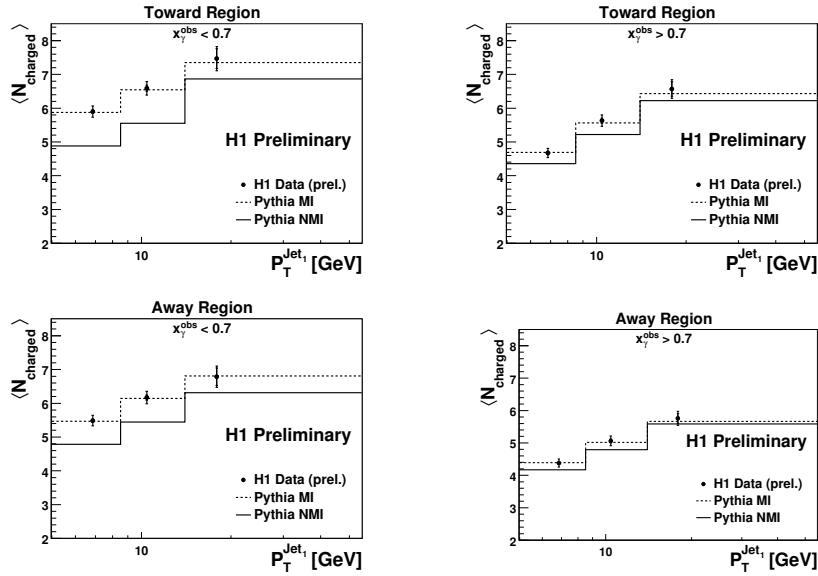


Figure 9: Charged particle multiplicity for  $x_\gamma < 0.7$  (left) and for  $x_\gamma > 0.7$  (right). Data is compared to PYTHIA MC predictions with and without multi-parton interactions.

- [6] S. Chekanov *et al.* [ZEUS Collaboration], JHEP **0906** (2009) 074, [arXiv:0812.2416 [hep-ex]].
- [7] H. Holtmann *et al.*, Phys. Lett. **B338** (1994) 363.
- [8] B. Kopeliovich, B. Povh and I. Potashnikova, Z. Phys. **C73** (1996) 125, [hep-ph/9601291].
- [9] M. Przybycień, A. Szczurek and G. Ingelman, Z. Phys. **C74** (1997) 509, [hep-ph/9606294].
- [10] A. Szczurek, N. N. Nikolaev and J. Speth, Phys. Lett. **B428** (1998) 383, [hep-ph/9712261].
- [11] L. Frankfurt, W. Koepf and M. Strikman, Phys. Lett. **B405** (1997) 367.
- [12] M. Grazzini, L. Trentadue, and G. Veneziano, Nucl. Phys. **B519** (1998) 394.
- [13] J.C. Collins, Phys. Rev. **D57** (1998) 3051; Erratum - *ibid.*, **D61** (2000) 019902.
- [14] J. Benecke *et al.*, Phys. Rev. **188** (1969) 2159.
- [15] T.T. Chou and C.N. Yang, Phys. Rev. **D50** (1994) 590.
- [16] N. N. Nikolaev, J. Speth and B. G. Zakharov, [hep-ph/9708290].
- [17] U. D’Alesio and H. J. Pirner, Eur. Phys. J. **A7** (2000) 109, [hep-ph/9806321].
- [18] V. A. Khoze, A. D. Martin and M. G. Ryskin, Eur. Phys. J. **C48** (2006) 797, [hep-ph/0606213].
- [19] J. D. Sullivan, Phys. Rev. **D5** (1972) 1732.
- [20] M. Bishari, Phys. Lett. **B38** (1972) 510.
- [21] K. Charchula, G. A. Schuler and H. Spiesberger, Comput. Phys. Commun. **81** (1994) 381, DJANGO 1.4.
- [22] H. Jung, Comp. Phys. Commun. **86** (1995) 147, RAPGAP 3.1.
- [23] C. Adloff *et al.* [H1 Collaboration], Eur. Phys. J. **C21** (2001) 33, [hep-ex/0012053].
- [24] M. Glück, E. Reya and I. Schienbein, Eur. Phys. J. **C10** (1999) 313, [hep-ph/9903288].
- [25] P. Aurenche *et al.*, Phys. Lett. **B233** (1989) 517.
- [26] T. Sjostrand and M. van Zijl, Phys. Rev. **D36** (1987) 2019.
- [27] T. Sjostrand, S. Mrenna and P. Skands, “PYTHIA 6.4 Physics and Manual,” JHEP **0605** (2006) 026, [hep-ph/0603175].
- [28] A. A. Affolder *et al.* [CDF Collaboration], Phys. Rev. **D65** (2002) 092002.
- [29] H1 Collaboration, “Study of Multiple Interactions In photoproduction at HERA”, H1prelim-08-036.